

Article

Mechanical Properties and Damage Evolution of Heated Granite Subjected to Liquid Nitrogen Cooling

Chunbo Zhou ¹, Feng Gao ^{1,*} , Chengzheng Cai ¹, Wenqi Zheng ² and Liupeng Huo ¹

¹ State Key Laboratory for Geomechanics and Deep Underground Engineering, China University of Mining and Technology, Xuzhou 221116, China

² School of Mechanics and Civil Engineering, China University of Mining and Technology, Xuzhou 221116, China

* Correspondence: jsppw@sohu.com

Abstract: To investigate the effect of liquid nitrogen on the granite failure process, the deterioration effect of liquid nitrogen on heated granite was investigated from experimental and theoretical perspectives. The mechanical properties of heated granite (25, 100, 200, 300, and 400 °C) after different cooling treatments (air cooling and liquid nitrogen cooling) were investigated by uniaxial compression tests. The damage evolution analysis was performed by a statistical damage constitutive model and the dissipation energy ratio was newly defined. The results show that there is an increase in the uniaxial compressive strength of heated granite before 200 °C, which is due to the competitive relationship between the thermal cracking and crack closure. Liquid nitrogen cooling can deteriorate the mechanical properties of heated granite in terms of strength and deformability. At 400 °C, the reduction rates of compressive strength and stiffness between air cooling and liquid nitrogen cooling reached 32.36% and 47.72%, respectively. Liquid nitrogen cooling induces greater initial thermal damage and, consequently, leads to a greater degree of total damage before the peak stress and makes rock easier to be damaged. At 400 °C, the total damage at the peak stress increased from 0.179 to 0.587 after the liquid nitrogen cooling. The difficulty of damage can be quantified by the dissipation energy ratio. In addition, the deterioration of liquid nitrogen on granite is positively related to temperature. This study confirmed the deterioration effect of liquid nitrogen and promoting effect of temperature, providing a theoretical approach to the degradation mechanism of liquid nitrogen.

Keywords: liquid nitrogen; degradation; statistical damage constitutive model; damage; dissipated energy ratio



Citation: Zhou, C.; Gao, F.; Cai, C.; Zheng, W.; Huo, L. Mechanical Properties and Damage Evolution of Heated Granite Subjected to Liquid Nitrogen Cooling. *Appl. Sci.* **2022**, *12*, 10615. <https://doi.org/10.3390/app122010615>

Academic Editor: Stefano Invernizzi

Received: 29 September 2022

Accepted: 17 October 2022

Published: 20 October 2022

Publisher's Note: MDPI stays neutral with regard to jurisdictional claims in published maps and institutional affiliations.



Copyright: © 2022 by the authors. Licensee MDPI, Basel, Switzerland. This article is an open access article distributed under the terms and conditions of the Creative Commons Attribution (CC BY) license (<https://creativecommons.org/licenses/by/4.0/>).

1. Introduction

The exploitation of geothermal energy is currently facing great challenges, as the utilization of geothermal energy is limited by the current fracturing capacity [1,2]. The efficiency of thermal extraction depends on the complexity of the fracture network [1]. The application of liquid nitrogen (LN₂) in fracturing engineering is being focused on and studied as a supplement or alternative to conventional hydraulic fracturing [3–6]. The low-temperature properties of LN₂ can lead to thermal stresses in contact with rock, especially high temperature rocks, which can induce thermal cracks within rock [7,8]. This can be very helpful in improving the efficiency of reservoir fracturing.

The degrading effect of LN₂ on the mechanical properties of rock is generally investigated experimentally. It has been demonstrated that LN₂ can degrade the mechanical properties of different types of rocks [9–11]. The sensitivity to LN₂ damage is different for rock types [11]. Especially, geothermal reservoir rocks have high temperature properties [2]. The mechanical properties of high temperature rock are different from those of room temperature rock [12–14]. The initial temperature of the rocks affects the degradation of LN₂ [15–17]. Benefiting from the current experimental means, the relationship between

the temperature and the degradation of LN₂ has been investigated objectively from various aspects. Many studies [15–18] found that the mechanical properties degraded by LN₂ can be enhanced with an increasing temperature. Especially over 400 °C, the degradation of LN₂ is obvious [16,17,19]. This is explained in that way that an increase in the initial temperature can enhance the induced thermal stress, and thus a more significant degradation effect [20]. In addition to the experimental means, numerical simulation is adopted to study the thermal treatment process [7,21,22] and reveals the positive correlation between the thermal damage and temperature in the process of LN₂ cooling. Current studies revealing the deterioration effect of LN₂ are mainly divided into two aspects: one is the mechanism of the initial damage caused by LN₂ [17,20,23,24], and the other is the mechanical behavior of rocks after the LN₂ damage [18,19,25]. The current studies mostly focus on the effect of LN₂ on mechanical parameters, such as porosity, P-wave velocity, strength, and peak strain. The effect of LN₂ on the whole failure process is not sufficient.

The mechanical behavior can be described as a constitutive model [26]. There are many approaches to building a constitutive model, such as the Neural network-based constitutive model [26], elastic damage constitutive model [27], and statistical damage constitutive model [28,29]. In the mesoscopic perspective, the mechanical parameters of rock matrixes can be regarded as satisfying a certain mathematical function distribution [30]. Assuming that the mechanical parameters of the rock matrix satisfy the Weibull distribution [31–33]. The failure process of rock is represented by the number of failure matrices; the number of failure matrices is calculated using the statistical method [30]. Combining the theory of continuum mechanics, the statistical damage constitutive model can be established. The statistical damage constitutive model has been widely adopted [32–34]. The damage evolution of rock can be analyzed by establishing a damage constitutive model. At present, investigating the degradation of LN₂ on rock by the damage constitutive model has not been focused on.

To help fill those gaps, the deterioration effect of LN₂ on heated granite was investigated from experimental and theoretical perspectives. The effect of LN₂ on the whole failure process was investigated by a statistical damage constitutive model. Through a damage evolution analysis and a newly defined energy parameter, the softening effect of LN₂ and the role of temperature were confirmed. This study provides a theoretical approach to the degradation mechanism of LN₂.

2. Materials and Methods

2.1. Materials Preparation and Experimental Procedure

2.1.1. Materials Preparation

The granite used in the experiment was obtained from Rizhao City. According to the uniaxial compression test in this study, the average density of the granite is 2654 kg/m³. The uniaxial compressive strength is 98 MPa. Young's modulus and Poisson's ratio are 20.04 GPa and 0.13. The specimens are 50 mm in diameter and 100 mm in height. The machining accuracy meets the ISRM standard [35]. To reduce the experimental discrete, all specimens are taken from the same rock, and the specimens with small differences in density and wave velocity are selected for further experiments.

In order to study the degradation of mechanical properties induced by LN₂ cooling, specimens cooled under natural conditions are used as the experimental control group. In order to investigate the relationship between the temperature and cooling degradation, five temperature levels (25, 100, 200, 300, and 400 °C) were set for the experiment. The experiment contains two parts (Figure 1): the thermal treatment and uniaxial compression test.

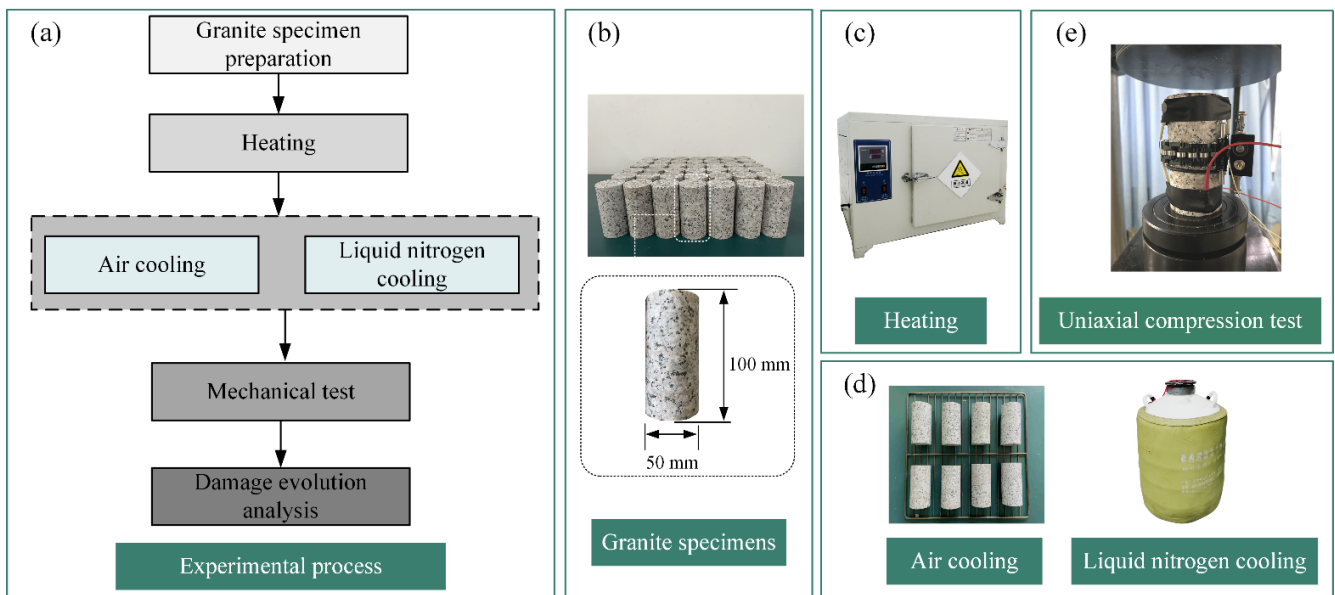


Figure 1. Experimental procedure.

2.1.2. Experimental Procedure

Before the uniaxial compression test, the specimens are heated to the target temperature and then cooled (Figure 2). The heating rate and maintenance time of the target temperature are 2–4 °C/min and 2 h [36]. After heating, specimens in the air-cooling group are placed in the air for cooling, and those of the LN₂-cooling group are immersed in LN₂ for cooling. When finishing cooling for 1 h, all specimens are placed under natural conditions for 24 h to ensure that all specimens can have subsequent mechanical property tests performed on them at the same temperature.

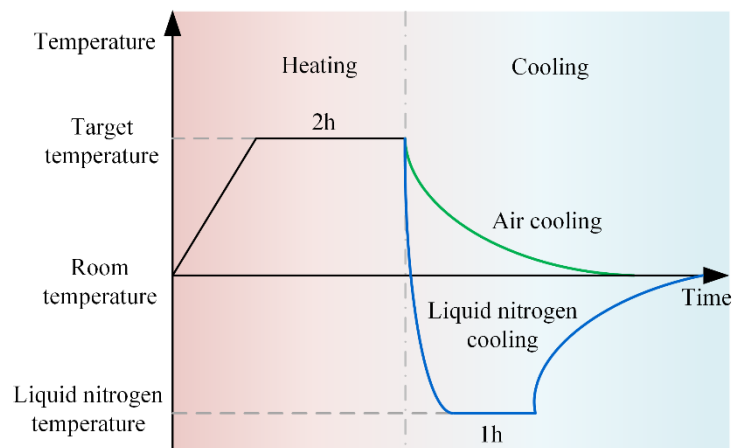


Figure 2. Thermal treatment schedule.

After the thermal treatment, the uniaxial compression test is performed by a TAW-2000 rock test system. Axial displacement is applied to the specimens at a rate of 0.2 mm/min until their failure. The axial stress, axial strain, and lateral strain are recorded and calculated.

2.2. Statistical Damage Constitutive Model

2.2.1. Damage Variables and Statistical Damage Constitutive Equation

The thermal damage variable D_T can be defined by Young’s modulus [17,33,37]:

$$D_T = 1 - \frac{E_T}{E_0} \tag{1}$$

where E_T is Young’s modulus after heating and cooling, and E_0 is Young’s modulus of the untreated rock.

The mechanical damage produced by loading is a continuous process, and mechanical damage can be used to describe the cumulative effect of the matrix damage under loading. Assuming that the strength of the rock matrix satisfied the Weibull distribution [31–33]:

$$P(\varepsilon) = \frac{m}{f_0} \left(\frac{f}{f_0}\right)^{m-1} \exp\left[-\left(\frac{f}{f_0}\right)^m\right] \tag{2}$$

where $P(\varepsilon)$ is the probability density function of the matrix strength, m and f_0 are the distribution parameters, and f is the strength variable of the rock matrix.

The total number of rock matrices is N , and the number of failure matrices is $N_f(f)$. The mechanical damage variable D_m is defined as [32,33]:

$$D_m = \frac{N_f(f)}{N} \tag{3}$$

The number of failure matrices in the interval $[0, f]$ can be calculated by Equation (2):

$$N_f(f) = \int_0^f NP(y)dy = N\left\{1 - \exp\left[-\left(\frac{f}{f_0}\right)^m\right]\right\} \tag{4}$$

Substituting Equation (4) into Equation (3), D_m is:

$$D_m = 1 - \exp\left[-\left(\frac{f}{f_0}\right)^m\right] \tag{5}$$

The maximum tensile strain yield criterion is assumed to determine the matrix strength [32,33], that is, $f = \varepsilon_1$. Equation (5) can be written as:

$$D_m = 1 - \exp\left[-\left(\frac{\varepsilon_1}{f_0}\right)^m\right] \tag{6}$$

According to the hypothesis of strain equivalence from Lemaitre [38], in uniaxial compression, the damage constitutive equation for heated granite after cooling the treatments is [32]:

$$\begin{cases} \sigma_1 = (1 - D_m)E_T\varepsilon_1 \\ E_T = (1 - D_T)E_0 \end{cases} \tag{7}$$

where σ_1 is the axial stress and ε_1 is the axial strain.

The total damage variable D is defined as the damage caused by the thermal treatments and loading. Equation (7) can be written as:

$$\begin{cases} \sigma_1 = (1 - D)E_0\varepsilon_1 \\ D = D_T + D_m - D_T D_m = 1 - \frac{E_T}{E_0} \exp\left[-\left(\frac{\varepsilon_1}{f_0}\right)^m\right] \end{cases} \tag{8}$$

2.2.2. Determination of m and f_0

The distribution parameters m and f_0 can be determined from the geometric properties of the experimental stress–strain curve. At the peak point of the stress–strain curve, the derivative of peak stress with respect to the strain is zero [32,33]:

$$\begin{cases} \varepsilon_1 = \varepsilon_p, \sigma_1 = \sigma_p \\ \varepsilon_1 = \varepsilon_p, \frac{d\sigma_1}{d\varepsilon_1} = 0 \end{cases} \tag{9}$$

where σ_p is the peak stress and ε_p is the strain corresponding to the peak stress.

Substituting Equation (9) into Equation (8), we get:

$$\sigma_p = \frac{E_T}{E_0} \exp \left[- \left(\frac{\varepsilon_1}{f_0} \right)^m \right] E_0 \varepsilon_p \tag{10}$$

$$E_T \exp \left[- \left(\frac{\varepsilon_p}{f_0} \right)^m \right] \left[1 - m \left(\frac{\varepsilon_p}{f_0} \right)^m \right] = 0 \tag{11}$$

We can derive from Equation (11):

$$\left(\frac{\varepsilon_p}{f_0} \right)^m = \frac{1}{m} \tag{12}$$

Combining Equations (12) and (10), we get:

$$\begin{cases} m = \frac{1}{\ln \frac{E_T \varepsilon_p}{\sigma_p}} \\ f_0 = \varepsilon_p m^{\frac{1}{m}} \end{cases} \tag{13}$$

According to the peak stress and its corresponding strain, the distribution parameters m and f_0 can be calculated by Equation (13), and the damage constitutive equation is determined by Equation (8).

2.3. Calculation of Energy Dissipation Ratio

The energy conservation of the rock failure process is [39]:

$$U = U_e + U_d \tag{14}$$

where U is the total energy absorbed by the rock, U_e is the elastic energy, and U_d is the dissipated energy.

In uniaxial compression, U can be calculated by:

$$U = \int_0^a \sigma_1 d\varepsilon_1 \tag{15}$$

where a is the upper limit of the integration, taking any moment strain.

U_e can be calculated by:

$$U_e = \frac{\sigma_1^2}{2E_0(1-D)} \tag{16}$$

where D is calculated by Equation (8).

Combining Equations (14)–(16), U_d can be calculated by:

$$U_d = U - U_e = \int_0^a \sigma_1 d\varepsilon_1 - \frac{\sigma_1^2}{2E_0(1-D)} \tag{17}$$

The evolution of damage is associated with energy dissipation. To demonstrate the difficulty of damage, the ratio of dissipated energy to damage is defined as the dissipation energy ratio α in this paper:

$$\alpha = \frac{U_d}{D} \tag{18}$$

3. Mechanical Properties of Heated Granite after Different Cooling Treatments

3.1. Stress–Strain Curves

The stress–strain curves of the specimens under different cooling treatments are shown in Figure 3. For a clear comparison, one typical curve of the specimens under the same conditions (same temperature and cooling method) is plotted in the figure. Compared with the specimens after air cooling (Figure 3a), the uniaxial compressive properties of the

specimens after LN₂ cooling (Figure 3b) are more obviously affected by the temperature. Above 200 °C (Figure 3c,d), the peak stress and Young's modulus after LN₂ cooling are generally lower than those after air cooling, and the lateral strain after LN₂ cooling is larger. The reduction in the peak stress indicates that the LN₂ treatment can make specimens easier to fail. The reduction of Young's modulus and the increase in lateral strains indicate that the LN₂ treatment can enhance the deformation properties, causing the softening effect, which is also founded by Hou et al. [15]. These results indicate that the LN₂ treatment can deteriorate the mechanical properties of granite, and the degradation is affected by the temperature. Therefore, the uniaxial compressive strength, Young's modulus, and Poisson's ratio will be compared in the following analysis to illustrate the degradation effect of LN₂ cooling on the mechanical properties of heated granite specimens.

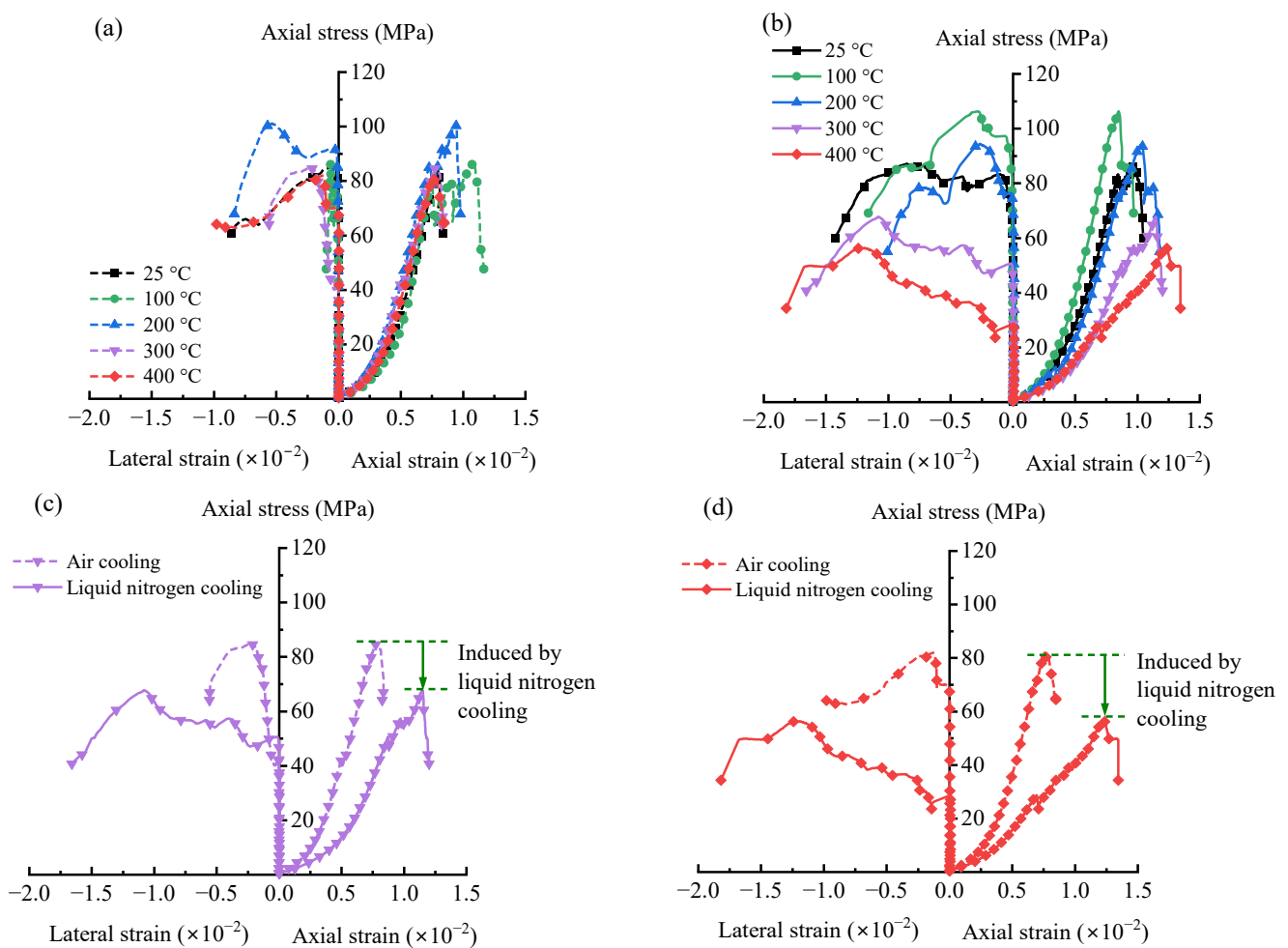


Figure 3. Stress–strain curves in uniaxial compression of specimens under: (a) air cooling and (b) liquid nitrogen cooling (c) at 300 °C and (d) at 400 °C.

3.2. Uniaxial Compressive Strength

The average compressive strength of the specimens under different cooling treatments is shown in Figure 4a. It can be seen from the curve of the air-cooling group that there is an increase in the strength before 200 °C, which is due to the competitive relationship between the thermal cracking and crack closure. The thermal cracking leads to a strength deterioration. However, the deformation of the mineral particles inside the specimen due to the temperature change leads to the closure of some of the cracks, which leads to a strength increase. The deformation of the crack closure is more prominent than thermal cracking when the temperature is moderate; at this time the increase in strength will occur. Above 200 °C (Figure 4a), the compressive strength decreases, which suggests that the

thermal cracking is more prominent. The critical temperature is where the mechanical transition from strengthening to weakening is related to the grain size distribution [12] and usually occurs below 500 °C [12,40]. The critical temperature declines with the increase in the heterogeneity of the grain size [12]. The coarse granite used in this study has a larger heterogeneity of grain size, leading to a lower critical temperature. From the LN₂-cooling group, there is also an increase in strength before 200 °C, but the strength after the LN₂ cooling is generally lower than that after the air cooling. After 200 °C, the compressive strength after the LN₂ cooling decreases significantly with the temperature increase and is significantly lower than that after the air cooling. The reduction rate of the compressive strength for LN₂ cooling compared with air cooling is given in Figure 4b. The reduction rate tends to improve with the increasing temperature, especially at 300 and 400 °C, the reduction rates reach 19.06% and 32.36%, respectively. These indicate that LN₂ cooling can deteriorate the compressive strength, and the deterioration is enhanced with the increasing temperature. The thermal damage is related to the temperature [7,21]. As the initial temperature increases, the temperature difference between the LN₂ and granite becomes larger. This leads to a larger temperature gradient and thermal deformation [7], which induces greater thermal stresses within the granite, and therefore the deterioration is more obvious.

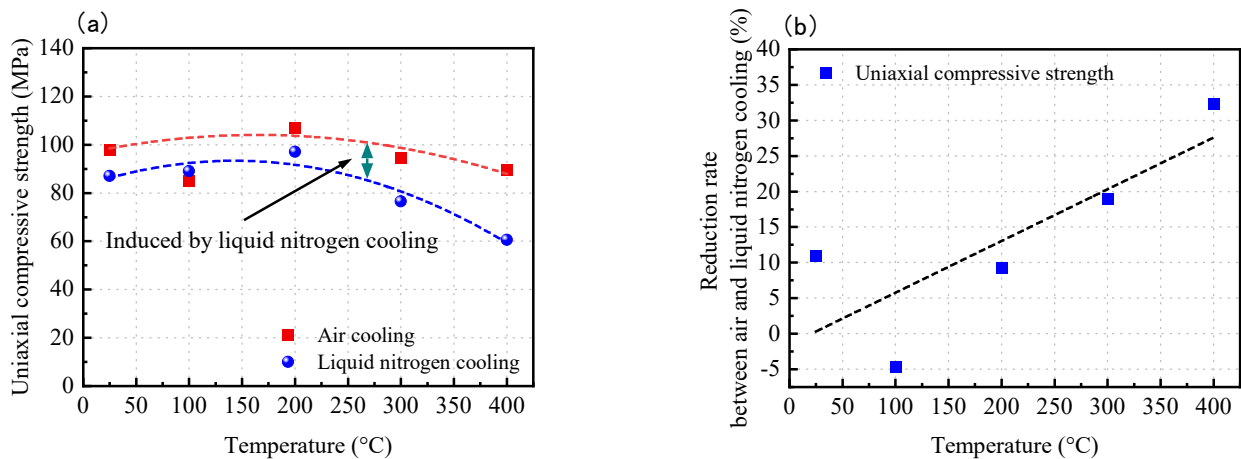


Figure 4. Effect of liquid nitrogen cooling on uniaxial compressive properties: (a) uniaxial compressive strength and (b) reduction rate of compressive strength between air and liquid nitrogen cooling.

3.3. Deformability in Uniaxial Compression

The average Young's modulus of the specimens under different cooling treatments is shown in Figure 5a. Young's modulus of the specimens after LN₂ cooling is lower than that after the air cooling, which indicates that the LN₂-cooling treatment can decrease the granite stiffness. Above 200 °C, the softening effect due to the LN₂ is more obvious. The reduction rate of Young's modulus for the LN₂ cooling compared with the air cooling is given in Figure 5b. The reduction rate is more significant with the increasing temperature. At 300 and 400 °C, the reduction rates reach 22.36% and 47.72%, respectively. These indicate that the softening effect due to the LN₂ is enhanced with the temperature. The softening effect of the LN₂ is also observed in Poisson's ratio. The LN₂-cooling treatment can increase Poisson's ratio (Figure 5c) and the increase rate by LN₂ is positively related to the temperature (Figure 5d), which suggests that the LN₂-cooling treatment can enhance the deformation properties and the improvement of deformability is more significant with the temperature. The increase in the initial temperature leads to a larger temperature difference between the LN₂ and granite. The larger the temperature difference, the greater the thermal-induced stresses within the granite, leading to a more obvious softening effect.

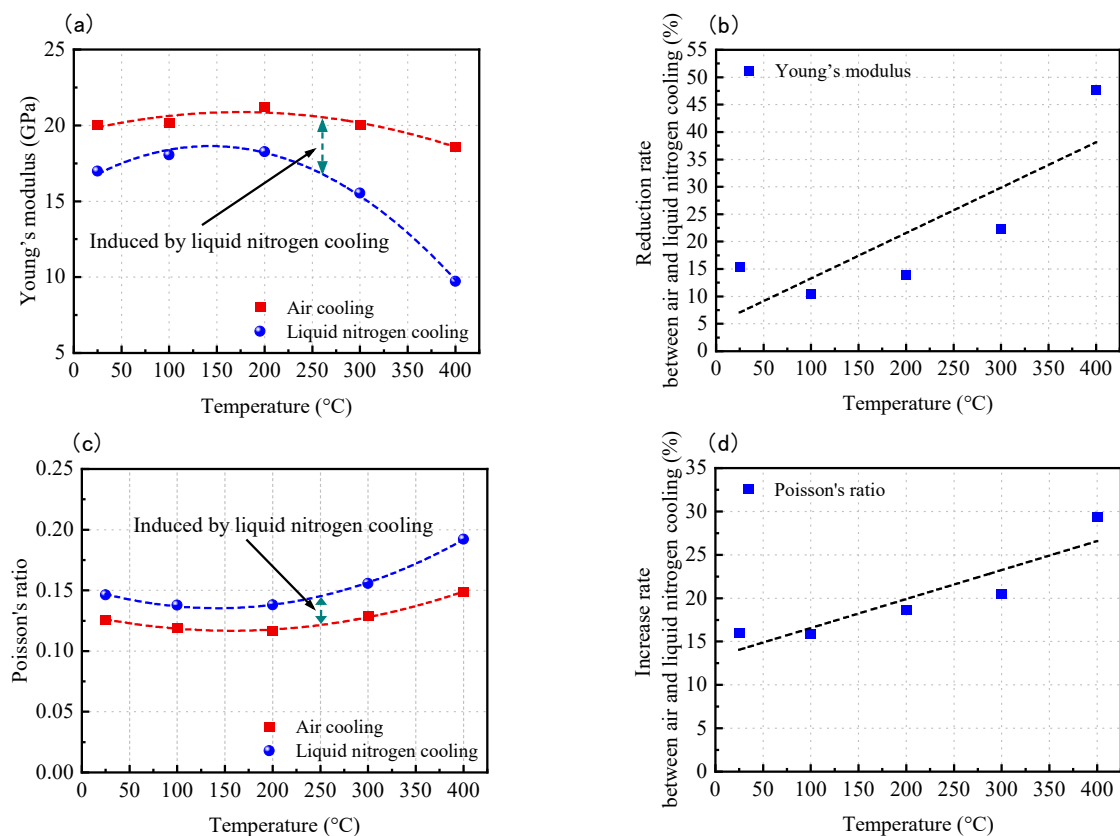


Figure 5. Effect of liquid nitrogen cooling on deformability: (a) Young's modulus, (b) reduction rate of Young's modulus between air and liquid nitrogen cooling, (c) Poisson's ratio, and (d) increase rate of Poisson's ratio between air and liquid nitrogen cooling.

4. Discussion on Damage Evolution

It is shown that the LN_2 treatment can deteriorate the mechanical properties of the heated granite in terms of strength and deformability, indicating that the LN_2 cooling can lead to damage to the granite. The stress–strain relationship reflects the mechanical behavior of the damage. The statistical damage constitutive model can describe the stress–strain relationship effectively and can be used for damage analysis [28]. Therefore, the damage evolution of granite under different cooling treatments is analyzed by a statistical damage constitutive model.

4.1. Model Validation

The statistical damage constitutive model (Equation (8)) has been widely adopted [32–34]. This model has been proved to describe the stress–strain relationships of rock [32,33]. For different types of rocks, Pan et al. [34] found that this model fitted well with hard rock with few voids, but it did not fit well with rock with high voids. This is because the current model cannot describe the void deformation during the initial compression stage. Granite is one kind of hard rock with few voids. Due to the thermal treatment, some cracks are induced within granite, which results in an obvious initial crack closure in the experimental stress–strain curves (Figure 6). Notably, the initial crack closure in the experimental stress–strain curves contains two forms of strain: the void deformation and elastic deformation of the rock matrix. It is assumed that the initial void deformation does not affect the damage evolution of the rock. The focus of our study is to analyze the damage evolution of granite. Thus, the void deformation is not considered in the established theoretical curve; the void deformation is subtracted from the experimental curve. The experimental and theoretical stress–strain curves for heated granite after different cooling treatments are shown in Figure 6. The theoretical curves are in a good agreement with the experimental

curves. On the one hand, the theoretical curves can accurately show the peak stress and its corresponding strain and can correctly reveal the effect of the temperature and cooling treatments on the stress–strain relationship. On the other hand, the theoretical curve can correctly describe the transformation from linear to nonlinear in the stress–strain curves, which successfully reflects the whole failure process: elasticity, damage, failure, and strain softening. The theoretical curves are in a good agreement with the experimental curves before the peak stress, which correctly reflects the damage behavior before the peak stress. The post-peak theoretical curves have a similar trend to the experimental curves, which can reveal the strain softening post-peak.

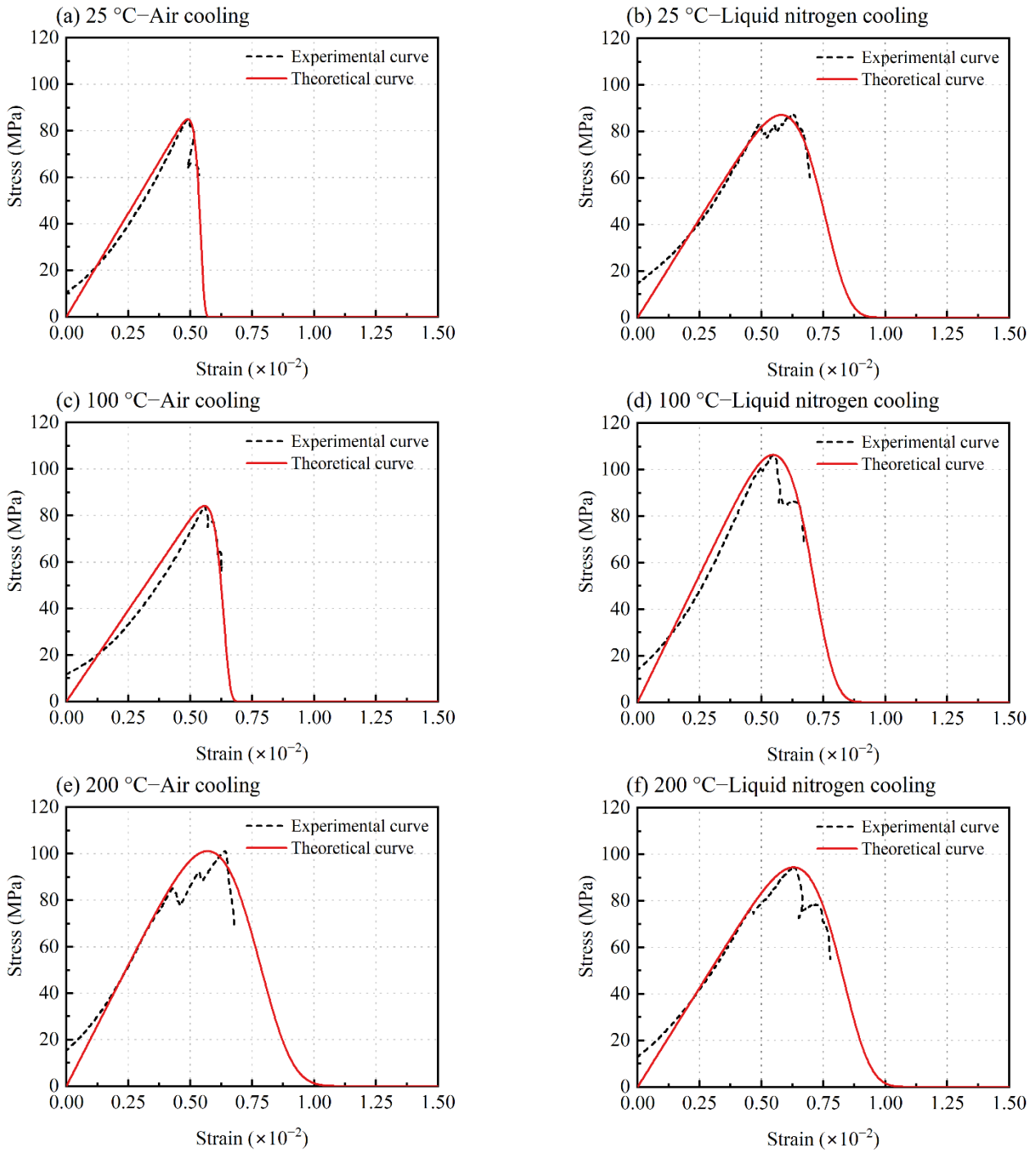


Figure 6. Cont.

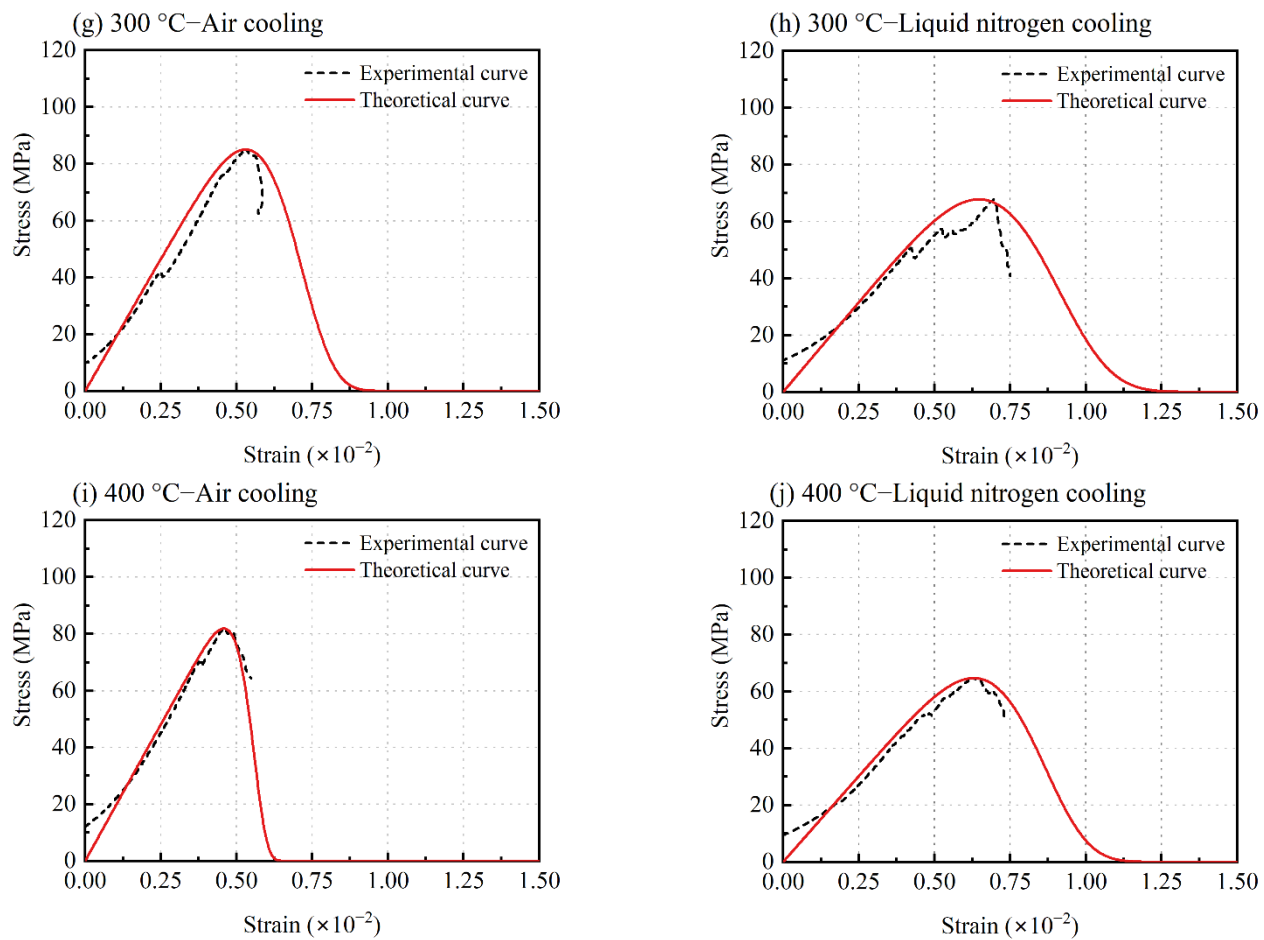


Figure 6. Experimental and theoretical stress–strain curves for heated granite after different cooling treatments.

The reason for the difference between the theoretical and experimental curves in that the post-peak is analyzed. Firstly, the granite used in the experiment is brittle and more likely to have sudden unstable failure after the peak stress, resulting in a large slope of the post-peak curve for certain specimens. The theoretical curves describe the cumulative effect of matrix damage and represent the ideal mode of failure, which leads to a smaller slope of the post-peak theoretical curves (Figure 6e,h). Secondly, sliding deformation occurs between the splitting cracks within uniaxial specimens before the failure (Figure 6b,e,h), however, the sliding deformation is not considered in the theoretical curves. This leads to a higher strain of failure than the theoretical value. The parameters of the theoretical curve are determined by the tested strain, and a higher tested strain results in a slower slope of post-peak theoretical curves. In order to improve the description accuracy of the uniaxial post-peak curve by the theoretical model, the peak strains of certain specimens are reduced and then used to calculate the theoretical curves. Specimens without a significant sliding deformation need not do so, and their tested strain can be used to directly determine the theoretical curves.

The distribution parameters m and f_0 of the theoretical model depend on the measured data. In order to reduce the dispersion of the measured data, the average values of the peak stress and strain under the same working conditions were adopted to calculate the distribution parameters and the damage constitutive model (Figure 7). The theoretical curves shown in Figure 7 are used in the following damage evolution analysis.

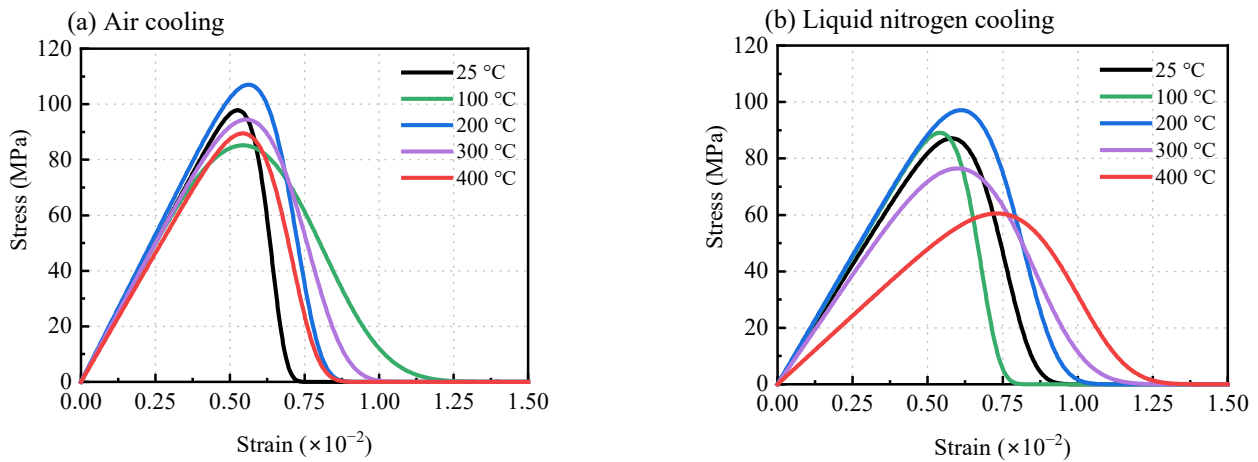


Figure 7. Theoretical stress–strain curves of heated granite after different cooling treatments (calculated by average value).

4.2. Damage Evolution Analysis

4.2.1. Damage Variable

The total damage variables are calculated by the second equation in Equation (8). The damage evolution of the heated granite after the different cooling treatments is shown in Figure 8. The total damage variables show an S-shaped trend with the increasing strain. The initial unchanged stage reveals the values of the thermal damage variables, where the mechanical damage variables are close to 0. The thermal damage variables increase significantly with the increasing temperature (especially at 300 and 400 °C), indicating that the temperature contributes to the increase in the thermal damage. The thermal damage variables are all higher after the LN₂ cooling than air cooling, indicating that the LN₂ cooling aggravates the degree of the thermal damage.

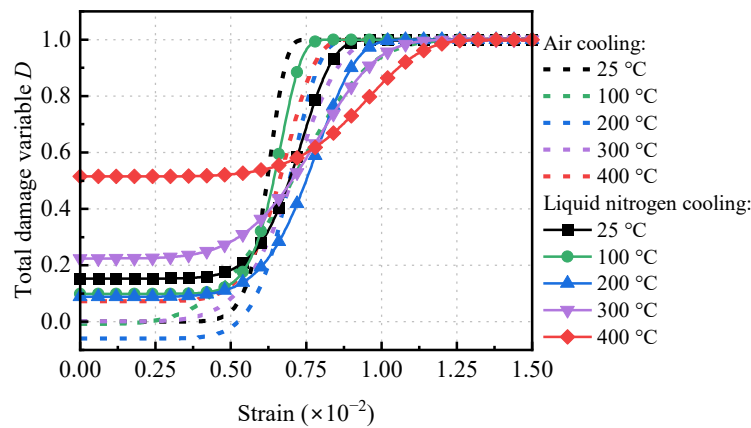


Figure 8. Total damage variables of heated granite after different cooling treatments.

To further analyze the damage evolution after the different cooling treatments, the specimens at 25, 200, and 400 °C are chosen for a specific analysis. To easily distinguish the pre- and post-peak damage curves, the strains are standardized by dividing them by the strains at the peak point. The total damage variable versus the normalized strain curves is presented in Figure 9. It can be found from the pre-peak curves that the total damage variables of the granite after the LN₂ cooling are all higher than the air cooling, which indicates that the LN₂ cooling induces a greater initial thermal damage and, consequently, leads to a greater degree of damage in the failure process. Comparing Figure 9a–c, the improvement in the total damage variables due to the LN₂ gradually increases with the increasing temperature. At 400 °C, the total damage at the peak stress increased from 0.179

to 0.587 after the LN₂ cooling. These indicate that the increase in temperature contributes to the thermal damage by the LN₂ cooling. From the post-peak curves, the slope of the damage variables after the LN₂ cooling is generally lower than that after the air cooling. The LN₂ cooling induces thermal cracks, which reduces rock brittleness and consequently makes rock “softer”.

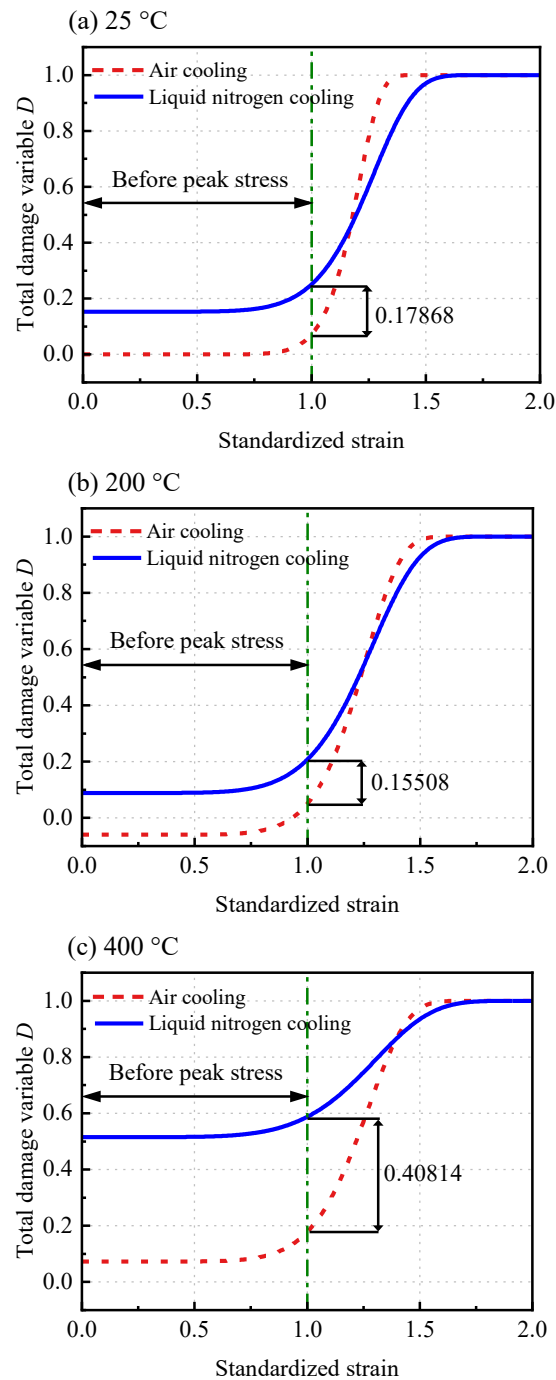


Figure 9. Total damage variables versus standardized strain.

4.2.2. Damage Evolution Rate

The damage evolution rate is the derivative of the total damaged variables with respect to the strain:

$$\frac{\partial D}{\partial \epsilon_1} = \frac{E_T}{E_0} \frac{m}{f_0} \left(\frac{\epsilon_1}{f_0}\right)^{m-1} \exp\left[-\left(\frac{\epsilon_1}{f_0}\right)^m\right] \quad (19)$$

The damage evolution rate versus the normalized strain curves is presented in Figure 10. The damage evolution rate can be divided into four stages: unchanged, increased, decreased, and unchanged. The initial stage represents the rock in the linear elastic stage, at this time the evolution rate is almost 0. The onset of an increase in the evolution rate represents the beginning of stable crack growth. The evolution rate increases significantly as the strain continues to increase; especially, the evolution rate increases rapidly after the peak stress. When numerous cracks coalesce and the rock bearing capacity decreases significantly, the evolution rate reaches a maximum. Afterwards, the evolution rate gradually decreases to 0. From the pre-peak curves, the increase in the evolution rate after the LN₂ cooling occurs earlier than that after the air cooling, indicating that granite is more easily damaged after the LN₂ cooling. From the post-peak curves, the evolution rate after the LN₂ cooling is generally lower than that after the air cooling, suggesting that LN₂ reduces the rock brittleness. Comparing Figure 10a–c, the damage evolution rate of granite after the LN₂ cooling gradually decreases with the increasing temperature. This means that the increasing temperature promotes the reduction in the brittleness due to LN₂, making the rock easier to be damaged.

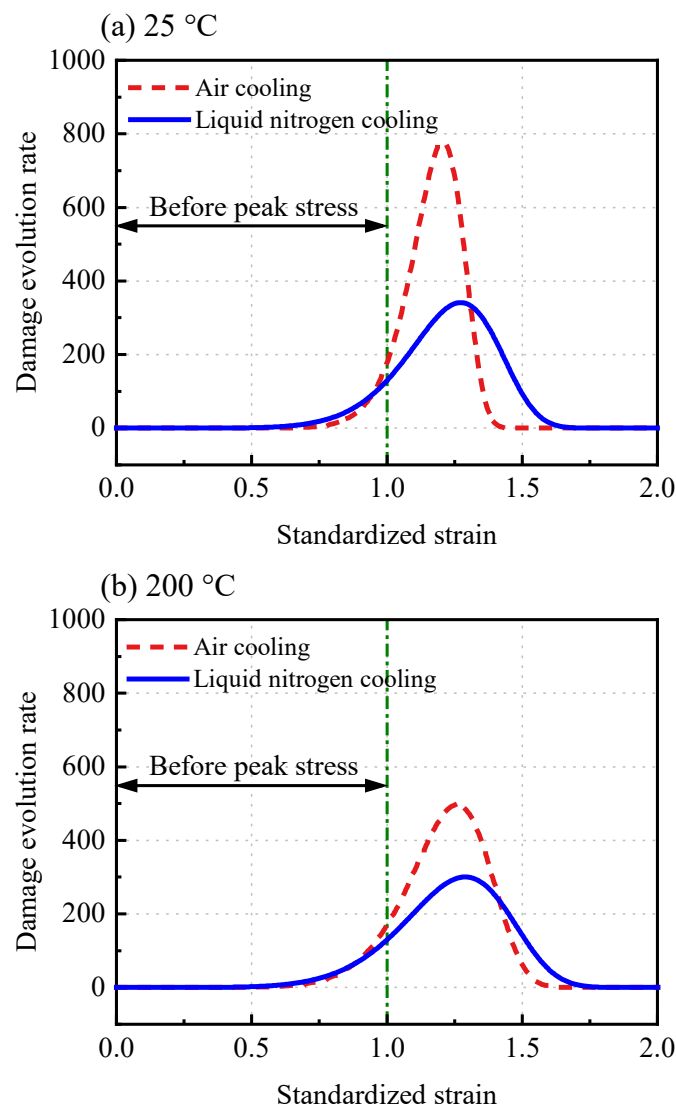


Figure 10. Cont.

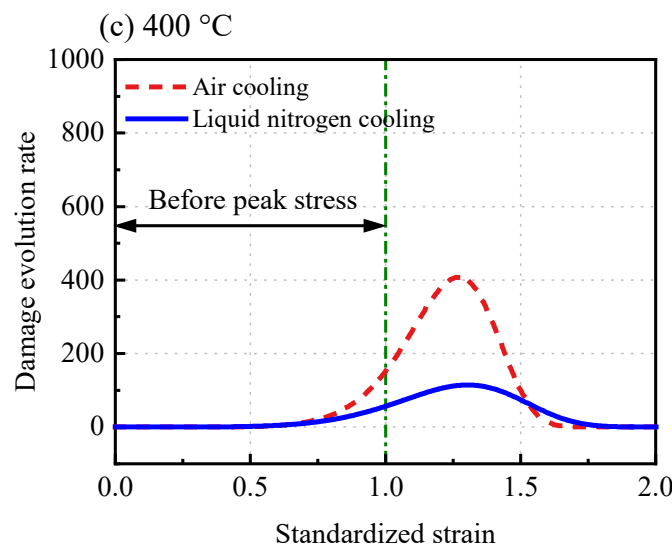


Figure 10. Damage evolution rate versus standardized strain.

4.2.3. Energy Dissipation Ratio

The dissipation energy at the peak stress can be calculated by Equation (17). It is found that the dissipation energy is discrete under the different temperatures and cooling methods. The dissipation energy is related not only to the damage degree but also to the difficulty degree of the damage. The damage degree is analyzed by the damage variable in Section 4.2.1. To demonstrate the difficulty degree of the damage, the dissipation energy ratio (Equation (18)) is defined and calculated. The smaller the energy dissipation ratio, the smaller the energy dissipation required to attain the same damage degree, suggesting that rock is more easily damaged. The energy dissipation ratio under different cooling treatments is shown in Figure 11. The energy dissipation ratio after the LN₂ cooling is lower than that after the air cooling, which indicates that rock is more easily damaged after the LN₂ cooling. At 200 °C, the air-cooled specimen has a maximum value, which is related to the improvement of the mechanical properties due to the crack closure during the heating process. However, the energy dissipation ratio is significantly reduced with the LN₂ cooling. The energy dissipation ratio after the LN₂ cooling is the lowest at 300 and 400 °C, indicating that high temperatures can promote the degradation of LN₂.

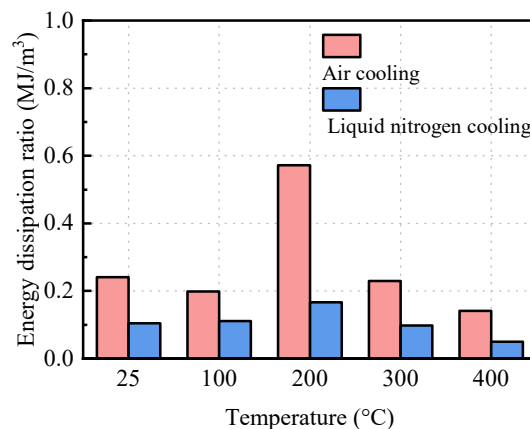


Figure 11. Effect of liquid nitrogen cooling on energy dissipation ratio.

4.3. Further Discussion on the Current Work

In this paper, it was found that the deterioration of LN₂ on granite is significantly affected by the temperature, and the deterioration effect is positively related to the temperature, which is also confirmed in the current studies [15–17]. LN₂ can not only deteriorate

mechanical parameters, but also affect the failure process [8]. At present, the failure process is mostly analyzed by acoustic emission techniques [17]; theoretical analysis is inadequate. To help fill those gaps, the statistical damage constitutive model [33] is adopted to describe the damage evolution. According to the derived damage variables and damage evolution rate, the softening effect [15] of LN₂ on granite is confirmed. In addition, the softening effect can be characterized by the difficulty of damage, which is quantified by the energy dissipation ratio newly defined in this paper. This study provides a theoretical approach to the degradation mechanism of LN₂.

In further studies, the statistical damage constitutive model adopted in this paper will be improved in several aspects. First, the initial void deformation was ignored in this study. The related works have focused on the void deformation in the literature [34,41]. The initial void deformation will be considered in the further model to make the model more reasonable. Second, different failure criterion types, such as the maximum tensile strain criterion [33], Mohr–Coulomb criterion [28], Drucker–Prager criterion [41], and Hoek–Brown criterion [29], are adopted to describe the matrix strength of the rock. The further model will choose a more reasonable strength criterion to determine the model parameters and improve the applicability of the model. Third, the model can be modified with the help of computer methods, such as the Neural network algorithm [26] and machine learning algorithm [42]. Finally, the damage constitutive model can be applied to numerical simulation analysis under complex working conditions.

5. Conclusions

Our study investigated the deterioration effect of LN₂ on heated granite from experimental and theoretical perspectives. The effect of LN₂ on the whole failure process was investigated by damage analysis. The softening effect of LN₂ on granite was confirmed. The role of the temperature in promoting a deterioration was revealed. The main conclusions are summarized below:

1. There is an increase in the uniaxial compressive strength of the heated granite before 200 °C, which is due to the competitive relationship between the thermal cracking and crack closure. When the temperature is high enough that the thermal cracking is more prominent, the compressive strength decreases.
2. The LN₂ cooling can deteriorate the mechanical properties of the heated granite in terms of strength and deformability. This softening effect is improved with the increasing temperature. At 400 °C, the reduction rates of the compressive strength and stiffness between the air cooling and LN₂ cooling reached 32.36% and 47.72%, respectively.
3. The LN₂ cooling induces greater initial thermal damage and, consequently, leads to a greater degree of total damage before the peak stress and makes rock easier to be damaged. The increase in temperature contributes to these deterioration effects. At 400 °C, the total damage at the peak stress increased from 0.179 to 0.587 after the LN₂ cooling.
4. Through the dissipation energy ratio, which was newly defined, the difficulty of the damage was revealed to characterize the softening effect of LN₂. It is proved that granite is more easily damaged after LN₂ cooling and a high temperature can promote the degradation of LN₂.

Author Contributions: Conceptualization, C.Z. and F.G.; methodology, C.Z.; validation, C.Z., F.G. and C.C.; investigation, W.Z. and L.H.; writing—original draft preparation, C.Z.; writing—review and editing, F.G.; supervision, F.G. All authors have read and agreed to the published version of the manuscript.

Funding: This work was supported by the National Natural Science Foundation of China (No. 51827901) and the National Key Research and Development Program of China (No. 2020YFA0711800).

Conflicts of Interest: The authors declare that there are no conflicts of interest.

References

1. Xie, H.; Li, C.; Zhou, T.; Chen, J.; Liao, J.; Ma, J.; Li, B. Conceptualization and evaluation of the exploration and utilization of low/medium-temperature geothermal energy: A case study of the Guangdong-Hong Kong-Macao Greater Bay Area. *Geomech. Geophys. Geo-Energy Geo-Resour.* **2020**, *6*, 18. [[CrossRef](#)]
2. Tomac, I.; Sauter, M. A review on challenges in the assessment of geomechanical rock performance for deep geothermal reservoir development. *Renew. Sustain. Energy Rev.* **2018**, *82*, 3972–3980. [[CrossRef](#)]
3. Grundmann, S.; Rodvelt, G.; Dials, G.; Allen, R. Cryogenic nitrogen as a hydraulic fracturing fluid in the Devonian Shale. In Proceedings of the SPE Eastern Regional Conference and Exhibition, Pittsburgh, PA, USA, 9–11 November 1998.
4. Mcdaniel, B.W.; Grundmann, S.; Kendrick, W.; Wilson, D.; Jordan, S. Field applications of cryogenic nitrogen as a hydraulic fracturing fluid. In Proceedings of the SPE Annual Technical Conference and Exhibition, San Antonio, TX, USA, 5–8 October 1997.
5. Yang, R.; Hong, C.; Liu, W.; Wu, X.; Wang, T.; Huang, Z. Non-contaminating cryogenic fluid access to high-temperature resources: Liquid nitrogen fracturing in a lab-scale Enhanced Geothermal System. *Renew. Energy* **2021**, *165*, 125–138. [[CrossRef](#)]
6. Zhang, S.; Huang, Z.; Zhang, H.; Guo, Z.; Wu, X.; Wang, T.; Zhang, C.; Xiong, C. Experimental study of thermal-crack characteristics on hot dry rock impacted by liquid nitrogen jet. *Geothermics* **2018**, *76*, 253–260. [[CrossRef](#)]
7. Su, S.; Hou, P.; Gao, F.; Liang, X.; Ding, R.; Cai, C. Changes in mechanical properties and fracture behaviors of heated marble subjected to liquid nitrogen cooling. *Eng. Fract. Mech.* **2022**, *261*, 108256. [[CrossRef](#)]
8. Zhou, C.; Gao, F.; Cai, C.; Wang, Z.; Zheng, W.; Gao, X. Integrating acoustic emission into a percolation model to evaluate crack distribution characteristics of heated granite subjected to rapid cooling. *Results Phys.* **2022**, *38*, 105600. [[CrossRef](#)]
9. Hou, P.; Xue, Y.; Gao, F.; Dou, F.; Su, S.; Cai, C.; Zhu, C. Effect of liquid nitrogen cooling on mechanical characteristics and fracture morphology of layer coal under Brazilian splitting test. *Int. J. Rock Mech. Min.* **2022**, *151*, 105026. [[CrossRef](#)]
10. Hou, P.; Chen, G.; Su, S.; Yang, Y.; Cai, C.; Wang, S.; Qiu, J.; Gao, F. Influence of various control factors on fracture toughness and fracture energy of sandstone subjected to liquid nitrogen cooling. *Energy Fuel.* **2022**, *36*, 397–406. [[CrossRef](#)]
11. Wu, X.; Huang, Z.; Zhang, S.; Cheng, Z.; Li, R.; Song, H.; Wen, H.; Huang, P. Damage analysis of high-temperature rocks subjected to LN₂ thermal shock. *Rock Mech. Rock Eng.* **2019**, *52*, 2585–2603. [[CrossRef](#)]
12. Kang, F.; Li, Y.; Tang, C. Grain size heterogeneity controls strengthening to weakening of granite over high-temperature treatment. *Int. J. Rock Mech. Min.* **2021**, *145*, 104848. [[CrossRef](#)]
13. Gautam, P.K.; Jha, M.K.; Verma, A.K.; Singh, T.N. Experimental study of thermal damage under compression and tension of Makrana marble. *J. Therm. Anal. Calorim.* **2020**, *139*, 609–627. [[CrossRef](#)]
14. Wang, F.; Frühwirt, T.; Konietzky, H. Influence of repeated heating on physical-mechanical properties and damage evolution of granite. *Int. J. Rock Mech. Min.* **2020**, *136*, 104514. [[CrossRef](#)]
15. Hou, P.; Su, S.; Zhang, Y.; Gao, F.; Gao, Y.; Liang, X.; Ding, R.; Cai, C. Effect of liquid nitrogen thermal shock on structure damage and brittleness properties of high-temperature marble. *Geomech. Geophys. Geo-Energy Geo-Resour.* **2022**, *8*, 69. [[CrossRef](#)]
16. Kang, F.; Jia, T.; Li, Y.; Deng, J.; Tang, C.; Huang, X. Experimental study on the physical and mechanical variations of hot granite under different cooling treatments. *Renew. Energy* **2021**, *179*, 1316–1328. [[CrossRef](#)]
17. Sha, S.; Rong, G.; Chen, Z.; Li, B.; Zhang, Z. Experimental evaluation of physical and mechanical properties of geothermal reservoir rock after different cooling treatments. *Rock Mech. Rock Eng.* **2020**, *53*, 4967–4991. [[CrossRef](#)]
18. Shao, Z.; Wang, Y.; Tang, X. The influences of heating and uniaxial loading on granite subjected to liquid nitrogen cooling. *Eng. Geol.* **2020**, *271*, 105614. [[CrossRef](#)]
19. Ge, Z.; Sun, Q.; Yang, T.; Luo, T.; Jia, H.; Yang, D. Effect of high temperature on mode-I fracture toughness of granite subjected to liquid nitrogen cooling. *Eng. Fract. Mech.* **2021**, *252*, 107834. [[CrossRef](#)]
20. Wu, X.; Huang, Z.; Song, H.; Zhang, S.; Cheng, Z.; Li, R.; Wen, H.; Huang, P.; Dai, X. Variations of physical and mechanical properties of heated granite after rapid cooling with liquid nitrogen. *Rock Mech. Rock Eng.* **2019**, *52*, 2123–2139. [[CrossRef](#)]
21. Zhou, C.; Gao, F.; Cai, C.; Su, S.; Zheng, W.; Huo, L. Variations in stress thresholds for heated granite subjected to rapid cooling under different confining pressures. *Nat. Resour. Res.* **2022**, *31*, 2653–2671. [[CrossRef](#)]
22. Wu, X.; Huang, Z.; Li, R.; Zhang, S.; Wen, H.; Huang, P.; Dai, X.; Zhang, C. Investigation on the damage of high-temperature shale subjected to liquid nitrogen cooling. *J. Nat. Gas Sci. Eng.* **2018**, *57*, 284–294. [[CrossRef](#)]
23. Sun, Y.; Zhai, C.; Xu, J.; Yu, X.; Cong, Y.; Zheng, Y.; Tang, W.; Li, Y. Damage and failure of hot dry rock under cyclic liquid nitrogen cold shock treatment: A non-destructive ultrasonic test method. *Nat. Resour. Res.* **2022**, *31*, 261–279. [[CrossRef](#)]
24. Rong, G.; Sha, S.; Li, B.; Chen, Z.; Zhang, Z. Experimental investigation on physical and mechanical properties of granite subjected to cyclic heating and liquid nitrogen cooling. *Rock Mech. Rock Eng.* **2021**, *54*, 2383–2403. [[CrossRef](#)]
25. Li, Q.; Yin, T.; Li, X.; Zhang, S. Effects of rapid cooling treatment on heated sandstone: A comparison between water and liquid nitrogen cooling. *Bull. Eng. Geol. Environ.* **2020**, *79*, 313–327. [[CrossRef](#)]
26. Cevik, A.; Sezer, E.A.; Cabalar, A.F.; Gokceoglu, C. Modeling of the uniaxial compressive strength of some clay-bearing rocks using neural network. *Appl. Soft Comput.* **2011**, *11*, 2587–2594. [[CrossRef](#)]
27. Tang, S.B.; Tang, C.A. Crack propagation and coalescence in quasi-brittle materials at high temperatures. *Eng. Fract. Mech.* **2015**, *134*, 404–432. [[CrossRef](#)]
28. Zhou, S.; Xia, C.; Zhao, H.; Mei, S.; Zhou, Y. Statistical damage constitutive model for rocks subjected to cyclic stress and cyclic temperature. *Acta Geophys.* **2017**, *65*, 893–906. [[CrossRef](#)]

29. Chen, Y.; Lin, H.; Wang, Y.; Xie, S.; Zhao, Y.; Yong, W. Statistical damage constitutive model based on the Hoek–Brown criterion. *Arch. Civ. Mech. Eng.* **2021**, *21*, 117. [[CrossRef](#)]
30. Rong, T.; Guan, C.; Liu, K.; Heng, S.; Shen, W.; Mou, R. A statistical damage constitutive model of anisotropic rock: Development and validation. *Geofluids* **2021**, *2021*, 6307895. [[CrossRef](#)]
31. Krajcinovic, D.; Silva, M.A.G. Statistical aspects of the continuous damage theory. *Int. J. Solids Struct.* **1982**, *18*, 551–562. [[CrossRef](#)]
32. Huang, S.; Liu, Q.; Cheng, A.; Liu, Y. A statistical damage constitutive model under freeze-thaw and loading for rock and its engineering application. *Cold Reg. Sci. Technol.* **2018**, *145*, 142–150. [[CrossRef](#)]
33. Fang, W.; Jiang, N.; Luo, X. Establishment of damage statistical constitutive model of loaded rock and method for determining its parameters under freeze-thaw condition. *Cold Reg. Sci. Technol.* **2019**, *160*, 31–38. [[CrossRef](#)]
34. Pan, Y.; Zhao, Z.; He, L.; Wu, G. A nonlinear statistical damage constitutive model for porous rocks. *Adv. Civ. Eng.* **2020**, *2020*, 8851914. [[CrossRef](#)]
35. Bieniawski, Z.T.; Bernede, M.J. Suggested methods for determining the uniaxial compressive strength and deformability of rock materials. *Int. J. Rock Mech. Min. Sci. Geomech. Abstr.* **1979**, *16*, 137–140. [[CrossRef](#)]
36. Kumari, W.G.P.; Ranjith, P.G.; Perera, M.S.A.; Chen, B.K.; Abdulagatov, I.M. Temperature-dependent mechanical behaviour of Australian Strathbogie granite with different cooling treatments. *Eng. Geol.* **2017**, *229*, 31–44. [[CrossRef](#)]
37. Chen, Y.; Xiao, P.; Du, X.; Wang, S.; Wang, Z.; Azzam, R. Study on damage statistical constitutive model of triaxial compression of acid-etched rock under coupling effect of temperature and confining Pressure. *Materials* **2021**, *14*, 7414. [[CrossRef](#)] [[PubMed](#)]
38. Lemaitre, J. How to use damage mechanics. *Nucl. Eng. Des.* **1984**, *80*, 233–245. [[CrossRef](#)]
39. Xie, H.; Li, C.; He, Z.; Li, C.; Lu, Y.; Zhang, R.; Gao, M.; Gao, F. Experimental study on rock mechanical behavior retaining the in situ geological conditions at different depths. *Int. J. Rock Mech. Min.* **2021**, *138*, 104548. [[CrossRef](#)]
40. Kumari, W.G.P.; Beaumont, D.M.; Ranjith, P.G.; Perera, M.S.A.; Avanthi Isaka, B.L.; Khandelwal, M. An experimental study on tensile characteristics of granite rocks exposed to different high-temperature treatments. *Geomech. Geophys. Geo-Energy Geo-Resour.* **2019**, *5*, 47–64. [[CrossRef](#)]
41. Wang, S.; Liao, H.; Chen, Y.; Fernández-Steegeer, T.M.; Du, X.; Xiong, M.; Liao, S. Damage evolution constitutive behavior of rock in thermo-mechanical coupling processes. *Materials* **2021**, *14*, 7840. [[CrossRef](#)] [[PubMed](#)]
42. Kurtoğlu, A.E.; Anil, Ö.; Çevik, A. A machine-learning-based constitutive bond-slip model for anchored CFRP strips externally bonded on concrete members. *Struct. Concr.* **2022**, *23*, 1828–1844. [[CrossRef](#)]